Experimental and Molecular Pathology 107 (2019) 129–140

Contents lists available at ScienceDirect

Experimental and Molecular Pathology

journal homepage: www.elsevier.com/locate/yexmp

Proteomic characterization of early lung response to breast cancer metastasis in mice

Anna Kurpińska[a], Joanna Suraj[a,b], Emilia Bonar[c], Agnieszka Zakrzewska[a], Marta Stojak[a], Magdalena Sternak[a], Agnieszka Jasztal[a], Maria Walczak[a,b,*]

[a] Jagiellonian University, Jagiellonian Centre for Experimental Therapeutics (JCET), Bobrzynskiego 14, 30-348 Krakow, Poland
[b] Jagiellonian University Medical College, Faculty of Pharmacy, Department of Toxicology, Medyczna 9, 30-688 Krakow, Poland
[c] Jagiellonian University, Faculty of Biochemistry, Biophysics and Biotechnology, Department of Analytical Biochemistry, Gronostajowa 7, 30-387 Krakow, Poland

ARTICLE INFO

Keywords:
Murine 4T1 model of breast cancer
Early lung metastasis
Biomarkers
Inflammation, oxidative stress
Pre-metastatic niche

ABSTRACT

Introduction: The tumor-promoting rearrangement of the lungs facilitates the process of cancer cell survival in a foreign microenvironment and enables their protection against immune defense. The study aimed to define the fingerprint of the early rearrangement of the lungs *via* the proteomic profiling of the lung tissue in the experimental model of tumor metastasis in a murine 4T1 mammary adenocarcinoma.

Materials and methods: The studies were performed on 7-8-week-old BALB/c female mice. Viable 4T1 cancer cells were orthotopically inoculated into the right mammary fat pad. The experiment was performed in the early phase of the tumor metastasis one and two weeks after cancer cell inoculation. The comparative analysis of protein profiles was carried out with the aid of the two-dimensional difference in gel electrophoresis (2D-DIGE). Proteins, of which expression differed significantly, were identified using nano-liquid chromatography coupled to a high-resolution mass spectrometry (nanoLC/hybrid ion trap- Orbitrap XL Discovery).

Results: Palpable primary tumors were noted in the 2nd week after cancer cell inoculation. The investigated period preceded the formation of numerous macrometastases in the lungs, however the metastasis-promoting changes were visible very early. Primary tumor-induced inflammation developed in the lungs as early as after the 1st week and progressed during the 2nd week, accompanied by increased concentration of 2-OH-E^{+}, an oxidative stress marker, and imbalance in nitric oxide metabolites, pointing to endothelium dysfunction. The early proteomic changes in the lungs in the 1st week after 4T1 cell inoculation resulted in the reorganization of lung tissue structure [actin, cytoplasmic 1 (Actb), tubulin beta chain (Tubb5), lamin-B1 (Lmnb1), serine protease inhibitor A3K (Serpina3k)] and activation of defense mechanisms [selenium-binding protein 1 (Selenbp1), endoplasmin (Hsp90b1), stress 70 protein, mitochondrial (Hspa9), heat shock protein HSP 90-beta (Hsp90ab1)], but also modifications in metabolic pathways [glucose-6-phosphate 1-dehydrogenase X (G6pdx), ATP synthase subunit beta, mitochondrial (Atp5b), L-lactate dehydrogenase B chain (Ldhb)]. Further development of the solid tumor after the 2nd week following cancer cell inoculation, secretion of prolific tumor-derived factors as well as the presence of the increasing number of circulating cancer cells and extravasation processes further impose reorganization of the lung tissue [Actb, vimentin (Vim), clathrin light chain A (Clta)], altering additional metabolic pathways [annexin A5 (Anxa5), Rho GDP-dissociation inhibitor 2 (Arhgdib), complement 1 Q subcomponent-binding protein, mitochondrial (C1qbp), 14-3-3 protein zeta/delta (Ywhaz), peroxiredoxin-6 (Prdx6), chitinase-like protein 4 (Chi3l4), reticulocalbin-1 (Rcn1), EF-hand domain-containing protein D2 (Efhd2), calumenin (Calu)]. Interestingly, many of differentially expressed proteins were involved in calcium homeostasis (Rcn1, Efhd2, Calu, Actb, Vim, Lmnb1, Clta, Tubb5, Serpina3k, Hsp90b1, Hsp90ab1, Hspa9. G6pdx, Atp5b, Anxa5, Arhgdib, Ywhaz).

Conclusion: The analysis enabled revealing the importance of calcium signaling during the early phase of metastasis development, early cytoskeleton and extracellular matrix reorganization, activation of defense mechanisms and metabolic adaptations. It seems that the tissue response is an interplay between pro- and anti-metastatic mechanisms accompanied by inflammation, oxidative stress and dysfunction of the barrier endothelial cells.

* Corresponding author at: Jagiellonian University, Jagiellonian Centre for Experimental Therapeutics (JCET), Bobrzynskiego 14, 30-348 Krakow, Poland.
E-mail addresses: anna.kurpinska@jcet.eu (A. Kurpińska), joanna.suraj@jcet.eu (J. Suraj), emilia.bonar@uj.edu.pl (E. Bonar), agnieszka.zakrzewska@jcet.eu (A. Zakrzewska), marta.stojak@jcet.eu (M. Stojak), magdalena.sternak@jcet.eu (M. Sternak), agnieszka.jasztal@jcet.eu (A. Jasztal), maria.walczak@jcet.eu (M. Walczak).

https://doi.org/10.1016/j.yexmp.2019.02.001
Received 14 October 2018; Received in revised form 25 January 2019; Accepted 9 February 2019
Available online 11 February 2019
0014-4800/

1. Introduction

Breast cancer is characterized by a robust ability to metastasize, specifically to the lungs (Weigelt et al., 2005). The architecture of the lung's small vessels facilitate the trapping of metastatic cancer cells (Langley and Fidler, 2011), however the formation of metastases also depends on a cross-talk between metastazing tumor cells and local non-tumor cells (Maru, 2015; Zheng et al., 2013). The primary tumor cells, in order to initiate pre-metastatic niche formation in the lungs, secrete numerous factors [*e.g.* vascular endothelial growth factor A (VEGFA), placental growth factor (PlGF), transforming growth factor-β (TGF-β), tumor necrosis factor-α (TNFα)], which alter the expression of proteins in the target organ [*e.g.*, stromal cell-derived factor 1 (SDF1), matrix metalloproteinases (MMPs), E-selectin] (Paget, 1989; Psaila and Lyden, 2009). These changes enable breaking the barrier of the endothelial cells (30% of lung cells), of which dysfunction facilitates the trapping of cancer cells and enables their extravasation (Blazejczyk et al., 2015; Crapo et al., 1982). In parallel, with the formation of a chemoattractive environment for metastazing tumor cells, the mediators released from primary tumor cells and affected lungs may stimulate the bone marrow-derived progenitor myeloid cells to produce suppressors of the immune response or stimulates the cells in the target organs to develop hematopoiesis. Both mechanisms lead to inflammatory infiltration. The presence of suppressors of the immune response (*e.g.*, tumor-associated macrophages (TAM), myeloid-derived suppressor cells, regulatory T cells) reduces the ability of organs to defend against cancer cells. What is more, active immune cells promote the development of a pro-inflammatory state, further extracellular matrix remodeling and thus metastatic niche formation and the generation of metastases (Jablonska et al., 2017; Quail and Joyce, 2013; Sceneay et al., 2013; Liu and Cao, 2016).

Despite considerable progress in diagnostics and pharmacotherapy, not fully understood mechanisms underlying metastasis development form barrier for the selection of an effective and selective treatment (Biemar and Foti, 2013). Genetic studies have a number of limitations, *e.g.*, expression profiles observed at the RNA level may differ significantly from those observed at the level of proteins. On the other hand, the studies conducted at the protein level are often limited to a single protein or specific group of proteins. Both may lead to false conclusions.

The selection of appropriate analytical methods, analysis of changes in the expression of protein repertoire (proteome) and analysis of the functional relationships between proteins permits the determination of potential biomarkers that can be used in targeted therapy (Weigelt et al., 2005). Newly developed targeted multibiomarker-oriented strategies are also a promising tool in the evaluation of disease progression (Walczak et al., 2015; Suraj et al., 2018; Suraj et al., 2019a).

Proteomic studies related to carcinogenesis and metastasis are numerous and include both the analysis of primary and metastatic tumors, as well as different tissues and biological fluids (Li et al., 2006; Ho et al., 2009; Kischel et al., 2008). Although, as noted by Brinton et al. (2012), there are many investigations concerning the early detection of cancer, not many deal with the definition of metastatic potential and particularly with characteristics of the metastatic processes. Further, these studies do not provide answers to the question of how the place of secondary tumor formation is selected. The 'seed and soil' hypothesis, introduced by Paget (1989), forwarded attention from the primary tumor characteristics and function to the properties of the target organs, which equally impose further tumor development. Yet, the factors released from primary tumors and the process of primary tumor development are well documented, but the early rearrangement of target organ function is still insufficiently comprehended.

For this reason the aim of this research was to investigate the mechanisms underlying the early rearrangement of the lungs and to detect the indicatory proteins characteristic of early metastasis-related formation of the tumor-promoting environment in the lungs within the experimental model of tumor metastasis in murine 4T1 mammary adenocarcinoma. A murine model of orthotopic 4T1 metastatic breast cancer was featured by the spontaneous, prolonged metastasis development from the primary tumor, which mimics the progression of the tumor in humans (Aslakson and Miller, 1992; Pulaski and Ostrand-Rosenberg, 2001; Bailey-Downs et al., 2014). The model allowed observation of early tissue remodeling and adaptation processes, which lead to the development of metastases in the target organ.

2. Material and methods

2.1. Materials and chemicals

The following reagents were purchased from Sigma-Aldrich (St. Louis, USA): ponceau xylidine, aniline blue, phosphotungstic acid hydrate, RPMI 1640 GlutaMAX medium, sodium pyruvate, antibiotic antimycotic solution (AAS), xylazine, methanol, dihydroethidium (DHE), acetonitrile (ACN), trifluoroacetic acid (TFA), MS-SAFE protease and phosphatase inhibitor (MS-SAFE PIC), acetone, DL-dithiothreitol (DTT), sodium dodecyl sulphate (SDS), glycerol, iodoacetamide (IAM), acetic acid (AcOH), sodium carbonate (Na_2CO_3), formaldehyde solution, ammonium bicarbonate (NH_4HCO_3). 10% fetal bovine serum (FBS) and Hanks Balanced Salt Solution (HBSS) were from Gibco, Life-Technologies (Waltham, USA). MycoAlert mycoplasma detection kit was produced by Lonza (Walkersville, USA). Ketamine was supplied by Vetoquinol (Gorzow Wielkopolski, Polska) and formaldehyde solution 4%, buffered, pH 7.4 was from Chempur (Piekary Slaskie, Poland). Tris Base and sequencing grade modified trypsin were purchased from Promega (Madison, USA) and urea, thiourea, [3-(3-cholamidopropyl) dimethylammonio]-1-propanesulfonate (CHAPS), agarose, Tris-Glycine-SDS buffer (TGS buffer) - 10x concentrate, sodium thiosulfate ($Na_2S_2O_2$) from BioShop (Burlington, Canada). Quick Start™ Bradford protein assay, ampholyte, IPG strips (17 cm, pH 4-7), stacking gel buffer 0.5 M Tris/HCl, pH 6.8, resolving gel buffer 1.5 M Tris-HCl, pH 8.8 were from Bio-Rad (Hercules, USA). Refraction-2D™ Labeling Kit was provided by ^{NH}DyeAGNOSTICS (Halle, Germany), 30% acrylamide/bis 37, 5:1 (2.6% C), silver nitrate ($AgNO_3$) and formic acid by VWR Chemicals (Radnor, USA) and ammonium persulfate (APS) with *N,N,N′,N′*-tetramethylethylenediamine (TEMED) by Amresco (Solon, USA). Potassium ferricyanide ($K_3FeC_6N_6$), acid fuchsin were purchased from Poch (Gliwice, Poland). Hematoxylin solution was ordered from Mar-Four (Konstantynow Lodzki, Poland).

2.2. Cell culture of the mouse mammary gland tumor cell line 4T1

A murine mammary carcinoma 4T1 cell line was purchased from American Type Culture Collection (ATCC, Manassas, USA) in 2015. Tumor 4T1 cells were cultured in RPMI1640 GlutaMAX medium with 10% FBS, AAS (20 units of penicillin, 20 mg streptomycin and 0.05 mg amphotericin B). Cells were maintained in T75 culture flasks at 37 °C in a humidified atmosphere (5% CO_2). Second passage was for inoculation of cancer cells into the mammary fat pad. Moreover, cells were regularly tested for mycoplasma contamination using the MycoAlert mycoplasma detection kit.

2.3. Murine model of metastatic breast cancer

Seven-to-eight-week-old BALB/c female mice were purchased from the Center for Experimental Medicine (Medical University of Bialystok, Poland). Mice had *ad libitum* access to water and were fed Altromin fodder. Tumor 4T1 cells were suspended in HBSS (1×10^4 cells/0.05 mL/mouse) and injected orthotopically into the right mammary fat pad. All analyses were performed one (1T) and two (2T) weeks after tumor cell inoculation (early metastatic period). Healthy BALB/c mice were employed as a control group (C). In order to confirm the development of the metastases in lungs in subsequent weeks of the

experiment (late metastatic period) the histology of the lungs was performed four weeks (4T) after 4T1 cell inoculation.

Experiments were conducted in accordance with ethical standards and according to the Declaration of Helsinki as well as national and international guidelines with approval by the authors' institutional review board. With this, all procedures were also approved by the I Local Ethical Committee for Experiments on Animals at the Jagiellonian University (Krakow, Poland).

Mice were anesthetized with a mixture of ketamine and xylazine at a concentration of 100 mg/mL and 10 mg/mL, respectively (0.025 mL of mixture/10 g body weight). Primary tumors were dissected from the surrounding tissues and measured with calipers. Thickness, width and length of the tumor were recorded. Weight of the lungs corrected to body mass was also noted.

2.4. Histopathological image analysis

Lung tissues [C (n = 10), 1T (n = 5), 2T (n = 6), 4T (n = 5)] were fixed in formaldehyde solution 4%, buffered, pH 7.4. Paraffin-embedded 5-μm sections (three sections per microscope slide) were stained with hematoxylin and eosin (H&E) and Masson Trichrome (Gray, 1954). Ten random images were taken at 200x for the assessment of inflammation, avoiding, if possible, the capture of subpleural large blood vessels and bronchi in order to capture exclusively the parenchyma, and additionally at 100x, 200x and 400x for visualization of metastases development. A light microscope Olympus BX51 (Olympus Corporation, Tokyo, Japan) was employed for digital recording of the sections.

2.5. Determination of nitric oxide metabolites in lung homogenates and plasma

For nitrite and nitrate determination lung homogenates [C (n = 14), 1T (n = 8) and 2T (n = 12)] and plasma [C (n = 24), 1T (n = 14) and 2T (n = 20)] were pelleted with methanol, centrifuged (14000 rpm, 10 min) and the supernatant was utilized for analysis immediately. The nitrite and nitrate concentration was assessed by a sensitive high-performance liquid chromatography-based technique (ENO-20 NOx Analyzer; EiCom, Kyoto, Japan) (Bryan and Grisham, 2007).

2.6. Determination of 2-hydroxyethidium (2-OH-E^+) in the lungs

Detection of 2-OH-E^+, a specific product of the superoxide (O_2^-) reaction with dihydroethidium (DHE) in tissues was performed according to a modified protocol described by Zielonka et al. (2008). A tissue section [C (n = 10), 1T (n = 7) and 2T (n = 12)] was incubated for 45 min with 10 μM DHE. Concentration of 2-OH-E^+ was evaluated by UFLC Nexera system (Shimadzu, Kioto, Japan) with fluorescence detection. Chromatographic separation was carried out on the analytical column Kinetex C18 (4.6 × 100 mm, 2.6 μm, Phenomenex, Torrance, USA) with the oven temperature set at 40 °C. The mobile phase consisted of acetonitrile (A) and water (B), both with an addition of 0.1% trifluoroacetic acid. The following linear eluting steps were included: 0.0 min (A:B, 25/75, v/v) - 0.5 min (A:B, 25/75, v/v) - 8 min (A:B, 35/65, v/v) - 9 min (A:B, 95/5, v/v) - 11 min (A:B, 95/5, v/v) - 12.0 min (A:B, 25/75, v/v) - 14.0 min (A:B, 25/75, v/v). The flow rate was set at 1 mL/min. A sample volume of 50 μL was injected onto column. The linearity range of the method was 0.005–0.5 μM.

2.7. Statistical analysis of biochemical data

Data are presented as the mean ± SEM. The assessment of normality (Shapiro-Wilk test) and equality of variances (Levene test) were conducted. To evaluate the statistical significance of the results, one-way analysis of variance (ANOVA) with Tukey's post-hoc test or non-parametric Kruskal-Wallis test were performed. The results were analyzed using Statistica 12.0 software (StatSoft, Tulsa, USA).

2.8. 2D-DIGE and gel image analysis

Two analyses were carried out for the comparison of the following groups: control *versus* 1T and 2T. Lung tissue samples were homogenized in sample buffer: 30 mM Tris Base, 7 M urea, 2 M thiourea, 4% CHAPS, MS-SAFE PIC (1:100) (pH 8.5) with Precellys Evolution Tissue Homogenizer (Bertin Technologies, France) (chilled with liquid nitrogen, 7500 rpm, 3 cycles, 30 s break). The homogenates were centrifuged (4 °C, 10000 *g*, 15 min) and 200 μL of supernatant was precipitated for two hours with ice-cold acetone (1:4). The samples were centrifuged (0 °C, 14000 *g*, 30 min), air dried and the pellet was dissolved in sample buffer. Protein concentration was determined with the aid of the Bradford method (Quick Start™ Bradford Protein Assay). Fluorescent dyes were prepared according to manufacturer's protocol (Refraction-2D™ Labeling Kit). Each gel was a mix of sample A (control, 50 μg of protein), sample B (1T or 2T, 50 μg of protein) and internal standard (IS) sample (50 μg of protein), thus total protein load was 150 μg. IS was prepared as follows: equal amount of proteins from all samples within the experiment were mixed and adjusted to 5 μg/μL. Each 50 μg of protein was labelled with the appropriate fluorescent dye: G-Dye200, G-Dye300 (samples A and B) and G-Dye100 (IS). The labelled samples, A, B and IS, were mixed (forming one gel set) and incubated for 15 min with equal volume of sample buffer supplemented with 130 mM DTT and 1% ampholyte (pH 3-10). Next, the rehydration buffer [sample buffer supplemented with 1% ampholyte (pH 3-10) and 130 mM DTT] was added to the total volume of 300 μL and loaded on IPG strips (17 cm, pH 4-7). IPG strips were actively rehydrated for 17 h at 20 °C and 50 V (PROTEAN® i12™ IEF System, Bio-Rad, Hercules, USA). Isoelectric focusing was performed as follows: (R - rapid voltage ramping mode, L - linear voltage ramping mode) 250 V, 300 Vh (R) → 500 V, 750 Vh (R) → 1000 V, 1500 Vh (R) → 5000 V, 2 h (L) → 5000 V, 90000 Vh (R): total 92550 Vh (Protean IEF, Bio-Rad, Hercules, USA) with a current limit of 50 μA per strip at 20 °C. Next, the proteins in the IPG strips were incubated in equilibration buffer (stacking gel buffer 0.5 M Tris/HCl, pH 6.8; 6 M urea, 2% SDS and 30% glycerol) with 1% DTT for 15 min, and for 20 min in 2.5% (*w/v*) iodoacetamide. SDS-PAGE was performed with 12% polyacrylamide gels [resolving gel buffer 1.5 M Tris-HCl, pH 8.8; 30% acrylamide/bis 37, 5:1 (2.6% C); 10% (w/v) SDS; 10% (w/v) ammonium persulfate; 1% TEMED; deionized water]. Molten agarose (0.5%) was employed to embed IPG strips on 12% gels. SDS-PAGE was performed in migration buffer [25 mM Tris; 192 mM; SDS 0.1% (w/v)]. SDS-PAGE was run at 10 °C at a stable parameter of 15 mA/gel, 1 W/gel, 40 V for 1 h, and 95 V for 18 h (Ettan DALTsix Large Vertical System, GE Healthcare, Chicago, USA). The obtained gel images were scanned using a Typhoon Trio + Scanner with 100 μm resolution (GE Healthcare, Chicago, USA). The filters were set to: G-Dye 100 (laser blue: 488 nm, filter: 620 nm BP40), G-Dye 200 (laser green: 532 nm, filter: 600 nm BP30), G-Dye 300 (laser red: 633 nm, filter: 580 nm BP30). Image analysis of gels was carried out using DeCyder 2D software v.7.2 (GE Healthcare, Chicago, USA). Twelve images were compared in each analysis. Differential in-gel analysis (DIA) was carried out with the estimated number of spots of 100000. Next, biological variation analysis (BVA) was applied with assignment to groups. The generated fold change and significance was manually checked for false positives. Statistical significance for each change was assessed using the Student's *t*-test. Spots were considered differentially expressed if the standardized average spot:volume ratio change reached the 95% confidence level (t-test p value < .05). Gels were silver-stained according to Shevchenko et al. (1996). Spots that significantly differed in expression (n = 3/protein) were manually excised from the gels and destined. Proteins were digested and peptides were extracted according to the protocol of Gundry et al. (2009). The obtained supernatants were dried in FreeZone 1 lyophilizer Labconco (Kansas, USA) and kept at −80 °C until analysis.

The lyophilizates were resuspended in 2% ACN in water (v/v) containing 0.1% FA (v/v). Dionex UltiMate™ 3000 RSLC System (Thermo Scientific, San Jose, USA) coupled to LTQ XL hybrid ion trap-Orbitrap Discovery mass spectrometer (Thermo Scientific, San Jose, USA) was used for proteomic analysis. After injection, peptides were trapped at 10 µL/min (Nano Trap Column, 100 µm *i.d.* × 20 mm, packed with Acclaim PepMap100 C18, 5 µm, 100 Å [loading phase consisted of 2% ACN in water (*v*/v) acidified with 0.1% FA (v/v)] and then separated on the analytical column (nanoViper column: 75 µm *i.d.* × 150 mm, packed with Acclaim PepMap RSLC C18, 2 µm, 100 Å). The column temperature was constantly set to 40 °C in the column oven. The mobile phases consisted of 0.1% FA in water (v/v) (A) and 0.1% FA in ACN (v/v) (B) were delivered in a gradient elution at the flow rate of 250 nL/min. Gradient elution was as follows: 2% B from 0 to 8 min, 2% - 5% B from 8 to 10 min, 5% - 35% B from 10 to 160 min, 35% - 90% B from 160 to 163 min, hold 90% B from 163 to 167 min, 90% - 2% B from 167 to 172 min and 20 min for column equilibration at 2% B. The total time of analysis was 192 min. The sample injection volume was 10 µL. The mass spectrometer was operated in data dependent mode. Full scan was performed from *m/z* 350–2000, with resolution set to 30000 FWHM (full width at half maximum) at 400 *m/z*. Eluting peptides were ionized at 1.8 kV. A top-eight method was used to select up to the eight most abundant precursor ions with a charge ≥2. Selected precursor ions were subjected to fragmentation on linear ion trap with collision-induced dissociation at a normalized collision energy of 35 (isolation width - 3 *m/z*, activation time - 30 ms, Q value of 0.25 and a minimum signal threshold of 1000 counts).

For protein identification, the Proteome Discoverer (version 1.4, Thermo Scientific, San Jose, USA) and MASCOT search engine (version 2.4.1, Matrix Science, London, UK) were used. The MS/MS-spectra were searched against the SwissProt database with the taxonomic restrictions to *Mus musculus* - 16973 sequences. The following parameters were set: enzyme - trypsin, taxonomy - *Mus musculus*, precursor mass tolerance - 10 ppm, fragment mass tolerance - 0.1 Da, 1 missed cleavage, fixed modifications - carbamidomethylation of cysteine, dynamic modifications - oxidation of methionine and false discovery rate - 1% ($p \leq .01$).

For the analysis of the functional relationships between the proteins that exhibited differences in expression various programs *e.g.*, String DB, Panther DB, GeneMania, GeneOnthology were used.

3. Results

3.1. Primary tumor development and histology of the lungs

The primary tumor was palpable in the right mammary fat pad during the 2nd week and reached after the 2nd week subsequent to cancer cell inoculation the following parameters: length - 5.52 mm ± 0.25 mm, thickness - 3.12 mm ± 0.19 and width - 5.58 mm ± 0.24 mm.

Lung weight corrected by body weight did not change between the control group (C - 0.0089 ± 0.0004) and the 1st and 2nd week after tumor cell inoculation (1T - 0.0085 ± 0.0004, 2T - 0.0089 ± 0.0002, respectively).

Histological analysis revealed that inflammation in the lungs developed during the 1st week after tumor inoculation and increased in the 2nd week (Fig. 1). Inflammation development was characterized by

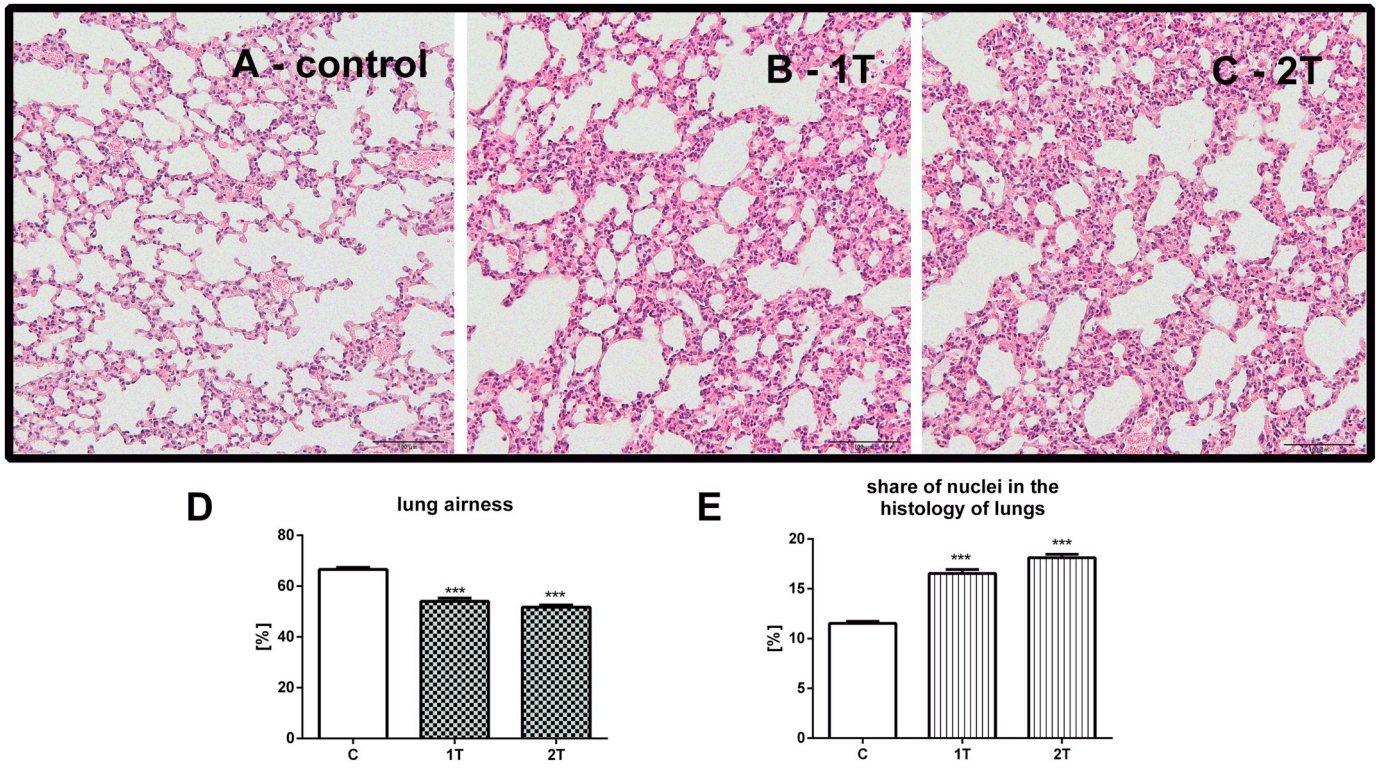

Fig. 1. Inflammation development in the lungs during the 4T1 mammary carcinoma progression. Gradual reduction in the area involved in direct gas exchange (alveolus, alveolar ducts, respiratory bronchioles) was noted despite an increase in alveolus volume. Restraints in respiratory surface result from increased infiltration of the cells and changes in extracellular matrix composition and congestion (A, B, C). Lung airness (D) - the share of the surface outside the tissue to the overall surface of the investigated section (%); share of the nuclei in the histology of lungs (E); share of the surface of the nuclei to the overall surface of the investigated section (%).

Legend: 1T ($n = 5$), 2T ($n = 6$) - weeks specified in each experimental group denote number of weeks after tumor cell inoculation. Healthy BALB/c mice were employed as a control group (Control, $n = 10$).

Representative images stained with H&E.

Magnification 200x (A, B, C).

an elevated number of inflammatory cells (increased number of nuclei in the histological section) as well as changes in extracellular matrix composition, transudations, edemas, hyperemias and hematomas, which result in reduced airness. Reduction in airness is defined as increased tissue volume to the detriment of the area involved in direct gas exchange (alveoles, alveolar ducts, respiratory bronchioles).

Although the tissue was significantly altered by inflammation, the histological analysis did not reveal macrometastases in the lungs within the first two weeks, however after careful analysis of the images, a few observed cells after the 2nd week exhibited cancer cell features and might be considered as potential metastatic cancer cells (early metastatic period) (Fig. 2). Additional histology of the lungs, 4 weeks after tumor cell inoculation confirmed afterward development of macrometastases.

3.2. Changes in the concentration of oxidative stress markers

In comparison to the control group the concentration of nitrites decreased in the lungs after the 1st week of the experiment and statistically lower values were also noted two weeks after tumor cell inoculation. Concentration of nitrates in lungs remained at a similar level throughout the experimental period. In plasma, statistically significantly lower nitrite values were noted after the 1st week of the experiment. Nitrates in plasma showed a similar tendency as for nitrites (a reduction following the 1st week) with a statistically significant elevation after the 2nd week (Fig. 3).

Analysis of oxidative stress markers in the lungs showed significant elevation of 2-OH-E$^+$ after the 1st, but this was also apparent after the 2nd week following tumor inoculation (Fig. 4).

3.3. Proteomic analysis of the early metastasis-related rearrangement of the lungs

One week after tumor cell inoculation, differences in expression were shown in 11 identified proteins (11 spots), whereas after the 2nd week in 15 protein spots, which were represented by 12 proteins. All differentially expressed proteins with details on identification statistics between the investigated groups were reported in Tables 1 and 2.

Reorganization of the structural components, including cytoskeleton, organelle organization and extracellular matrix remodeling was noted [actin, cytoplasmic 1 (Actb), tubulin beta chain (Tubb5), lamin-B1 (Lmnb1), serine protease inhibitor A3K (Serpina3k), vimentin

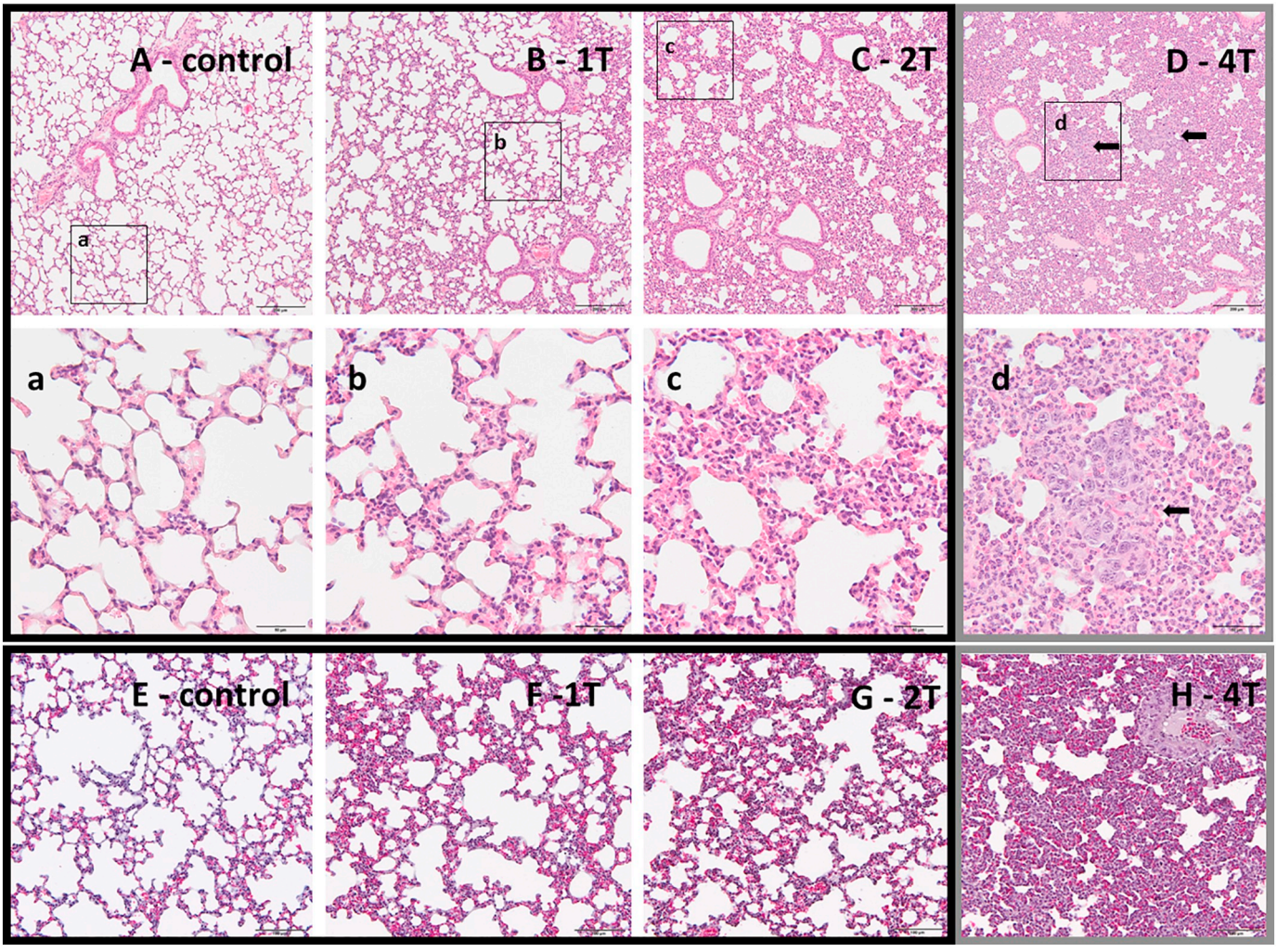

Fig. 2. Histological analysis of early and late metastatic lungs.
The early metastatic period (1T - B, b, F and 2T - C, c, G) was characterized by inflammation, hyperemia, reduction in alveolar volume related to the onset of metastasis development in the lungs. The observed changes underlie the development of the macrometastases in the following weeks of the experiment (4T - D, d, H).
Legend: 1T (n = 5), 2T (n = 6), 4T (n = 5) - weeks specified in each experimental group denote number of weeks after tumor cell inoculation. Healthy BALB/c mice were employed as a control group (Control - A, a, E, n = 10).
Representative images stained with H&E (A, B, C, D, a, b, c, d) and Masson Trichrome (E, F, G, H).
Magnification 100x (A, B, C, D) + 400x (a, b, c, d); 200x (E, F, G, H).

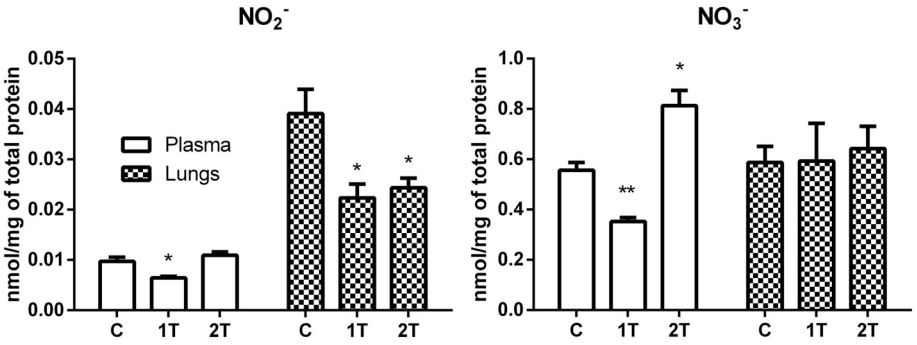

Fig. 3. Changes in the concentration of NO metabolites (nitrites, nitrates) in plasma and lungs.
Legend: 1T, 2T - weeks specified in each experimental group denote number of weeks after tumor cell inoculation, C - control group; lung homogenates - C (n = 14), 1T (n = 8) and 2T (n = 12), plasma - C (n = 24), 1T (n = 14) and 2T (n = 20).
Statistically significant changes are marked to control group: * $p < .05$, ** $p < .01$; data are represented as mean ± SEM.

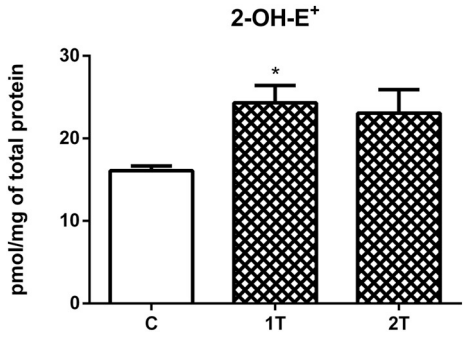

Fig. 4. Oxidative stress in the lungs. Changes in 2-OH-E^+ concentration in the lungs during the early metastatic period.
Legend: 1T (n = 7), 2T (n = 12) - weeks specified in each experimental group denote number of weeks after tumor cell inoculation, C - control group (n = 10).
Statistically significant changes are marked to control group: * $p < .05$; data are represented as mean ± SEM.

(Vim), clathrin light chain A (Clta)]. Multiple processes were altered, including immunological defense [selenium-binding protein 1 (Selenbp1), endoplasmin (Hsp90b1), stress 70 protein, mitochondrial (Hspa9), heat shock protein HSP 90-beta (Hsp90ab1)], metabolic pathways [glucose-6-phosphate 1-dehydrogenase X (G6pdx), ATP synthase subunit beta, mitochondrial (Atp5b), L-lactate dehydrogenase B chain (Ldhb), annexin A5 (Anxa5), Rho GDP-dissociation inhibitor 2 (Arhgdib), complement 1 Q subcomponent-binding protein, mitochondrial (C1qbp), 14-3-3 protein zeta/delta (Ywhaz), peroxiredoxin-6 (Prdx6), chitinase-like protein 4 (Chi3l4), reticulocalbin-1 (Rcn1), EF-hand domain-containing protein D2 (Efhd2), calumenin (Calu) (Fig. 5).

Interestingly, many of the differentially expressed proteins were involved in calcium homeostasis like Rcn1, Efhd2, Calu, Actb, Vim, Lmnb1, Clta, Tubb5, Serpina3k, Hsp90b1, Hsp90ab1, Hspa9, G6pdx, Atp5b, Anxa5, Arhgdib and Ywhaz, underlying the importance of calcium signaling in the process of tumor development.

After the 1st week subsequent to cancer cell inoculation structural changes, modifications to the organization/localization of cellular components were seen. The changes were noted for Actb, Lmnb1, Tubb5 and Serpina3k, whereas after the 2nd week, Vim and Clta were modified.

The proteins that reflected altered metabolic processes *e.g.* binding, catalytic activity were represented after the 1st week of the experiment by G6pdx, Ldhb and Atp5b, and after the 2nd week by Anxa5, C1qbp, Prdx6 and Chi3l4, Ywhaz, Arhgdib, Calu, Efhd2 and Rcn1.

As early as after the 1st week of the experiment, changes in defense mechanisms were observed in Hsp90ab1, Hsp90b1, Hspa9 and Selenbp1.

4. Discussion

4.1. Assessment of disease progression

Murine models of spontaneously metastasizing 4T1 mammary gland carcinoma with prolonged development of metastasis were chosen for the studies of early metastatic rearrangement of the lungs (Suraj et al., 2019b; Buczek et al., 2018; Bailey-Downs et al., 2014; Smeda et al., 2018). During these investigations, the number of inoculated cancer cells was low, resulting in late development of metastases. The primary tumors were detected in the right mammary gland during the 2nd week after tumor cell inoculation and increased in subsequent weeks (Suraj et al., 2019b).

The histopathological analysis of the lungs uncovered the early rebuilding of the tissue. The concomitant inflammation induced by the presence of the tumor cells developed in lungs as early as one week after inoculation, progressed during the 2nd week, and was characterized by the reduction in alveolar volume, increased number of erythrocytes, enhanced extracellular matrix and infiltration of leucocytes (Fig. 1). The application of the algorithm that calculates the ratio between tissue volume (nuclei, cytoplasm, exudations) and empty space (air volume) enabled assessment of the properties of the tissue. Although the algorithm does not differentiate between the particular types of observed cells, it allows assessing the airness and infiltration of the immune cells. In the presented studies, lung airness was decreased after the 1st and 2nd week of the study when compared with control lungs, which was accompanied by increased infiltration of the immune cells (Fig. 1C-D) and greater extracellular matrix volume. Described inflammatory changes formed the environment for metastasis development. Neutrophils entering the lungs destabilize the bonds between endothelial cells and excrete elastase to force beyond the basal membrane and enter the lung parenchyma. This process results in greater settlement of the tumor cells (Dorweiler et al., 2008; Powell and Huttenlocher, 2016). Importantly, the presence of the numerous immunological suppressor cells indicates quiescence of the immunological response of healthy lung cells (Quail and Joyce, 2013).

Although the macrometastases were not detected by histopathological analysis of the lungs 1 and 2 weeks after the injection of tumor cells (Fig. 2), the onset of metastasis-related changes was supported by the progression of inflammation and changes in other investigated parameters. As evidenced in the histology of the 4th week, the changes finally led to the development of metastases. Indeed, the other studies in this model confirmed that micrometastases were formed around the investigated period and preceded the development of numerous macrometastases (Suraj et al., 2019b; Smeda et al., 2018; Chrabaszcz et al., 2018). Thus, the changes in the lungs in the first two weeks after tumor inoculation strictly underlie further development of metastases.

4.2. Early metastatic rearrangement of the lungs - proteomic considerations

Despite considerable progress in characterization of cancer development, proteomic studies related to the formation of metastases focus

Table 1
Proteins which showed differences in expression between control group and 1st week after inoculation of cancer cells.

Accession	Description	Score	Coverage	Proteins	Unique peptides	Peptides	PSMs	AAs	MW [kDa]	Calc. pI	t-student (*p*)	Average ratio	In 1T
P99024	Tubulin beta-5 chain GN = Tubb5	910.06	40.09%	7	11	13	25	444	49.6	4.89	0.037	1.15	Downregulation
P60710	Actin, cytoplasmic 1 GN = Actb	3419.49	58.67%	3	8	20	96	375	41.7	5.48	0.023	1.13	Downregulation
P60710	Actin, cytoplasmic 1 GN = Actb	798.16	29.87%	3	2	12	25	375	41.7	5.48	0.037	1.11	Downregulation
P08113	Endoplasmin GN = Hsp90b1	7400.27	56.73%	2	58	61	238	802	92.4	4.82	0.043	1.14	Upregulation
P11499	Heat shock protein HSP 90-beta GN = Hsp90ab1	2794.52	47.24%	5	18	33	75	724	83.2	5.03	0.034	1.16	Upregulation
P60710	Actin, cytoplasmic 1 GN = Actb	804.71	40.80%	3	4	13	28	375	41.7	5.48	0.0092	1.18	Downregulation
P56480	ATP synthase subunit beta, mitochondrial GN = Atp5b	2596.76	55.01%	1	20	20	55	529	56.3	5.34	0.031	1.14	Upregulation
P16125	L-lactate dehydrogenase B chain GN = Ldhb	746.76	29.64%	3	11	11	18	334	36.5	6.05	0.011	1.23	Downregulation
P38647	Stress-70 protein, mitochondrial GN = Hspa9	2753.33	45.21%	1	26	27	58	679	73.4	6.07	0.021	1.39	Downregulation
P07759	Serine protease inhibitor A3K GN = Serpina3k	1455.38	33.25%	6	13	13	28	418	46.8	5.16	0.028	1.43	Downregulation
P14733	Lamin-B1 GN = Lmnb1	3806.25	62.76%	3	48	48	96	588	66.7	5.16	0.015	1.16	Downregulation
Q00612	Glucose-6-phosphate 1-dehydrogenase X GN = G6pdx	1131.26	40.00%	2	24	24	35	515	59.2	6.49	0.05	1.12	Downregulation
P17563	Selenium-binding protein 1 GN = Selenbp1	5239.25	61.02%	2	25	25	122	472	52.5	6.29	0.024	1.12	Downregulation

Legend: 1T - one week after tumor cells inoculation.
Accession: UniProt number.
Description: Details about the protein including: name of the protein, gene name.
Score: Total score of the protein. This score is the sum of the scores of the individual peptides.
Coverage: The percentage of the protein sequence covered by identified peptides.
Proteins: The number of identified proteins in the protein group of a master protein.
Unique peptides: The number of peptide sequences unique to a protein group.
Peptides: The number of unique peptide sequences.
PSMs: The total number of identified peptide sequences (peptide spectrum matches) for the protein, including those redundantly identified.
AAs: The sequence length of the protein.
MW: The calculated molecular weight of the protein.
Calc. pI: The theoretically calculated isoelectric point.
Average ratio: The ratio between the volumes of the spot between the compared images.

Table 2
Proteins which showed differences in expression between control group and 2nd week after inoculation of cancer cells.

Accession	Description	Score	Coverage	Proteins	Unique peptides	Peptides	PSMs	AAs	MW [kDa]	Calc. pI	t-student (*p*)	Average ratio	In 2T
P48036	Annexin A5 GN = Anxa5	2656.17	71.79%	1	25	25	63	319	35.7	4.96	0.046	1.35	Upregulation
O35658	Complement component 1 Q subcomponent-binding protein, mitochondrial GN = C1qbp	1799.44	44.96%	1	6	6	39	278	31.0	4.92	0.0056	1.38	Downregulation
P63101	14-3-3 protein zeta/delta GN = Ywhaz	3828.98	72.65%	3	17	24	121	245	27.8	4.79	0.023	2.60	Upregulation
Q61599	Rho GDP-dissociation inhibitor 2 GN = Arhgdib	1895.49	82.50%	1	16	16	65	200	22.8	5.11	0.00098	2.08	Upregulation
O08585	Clathrin light chain A GN = Clta	860.08	27.66%	2	12	12	29	235	25.6	4.58	0.005	1.41	Downregulation
O08709	Peroxiredoxin-6 GN = Prdx6	2703.56	79.91%	1	21	21	76	224	24.9	6.01	0.032	1.12	Downregulation
P20152	Vimentin GN = Vim	5264.39	75.97%	10	43	46	131	466	53.7	5.12	0.038	1.08	Downregulation
O35887	Calumenin GN = Calu	2185.14	60.00%	1	16	16	53	315	37.0	4.67	0.021	1.25	Downregulation
O35887	Calumenin GN = Calu	2564.28	60.63%	1	20	20	73	315	37.0	4.67	0.03	1.27	Downregulation
P60710	Actin, cytoplasmic 1 GN = Actb	1214.90	60.00%	3	6	19	40	375	41.7	5.48	0.045	1.15	Downregulation
Q91Z98	Chitinase-like protein 4 GN = Chil4	1088.38	44.53%	2	12	12	23	402	44.9	6.19	0.028	1.16	Downregulation
P63101	14-3-3 protein zeta/delta GN = Ywhaz	3456.69	82.04%	3	17	26	95	245	27.8	4.79	0.0034	2.96	Upregulation
Q9D8Y0	EF-hand domain-containing protein D2 GN = Efhd2	875.20	41.67%	2	11	11	20	240	26.8	5.06	0.017	3.32	Upregulation
Q05186	Reticulocalbin-1 GN = Rcn1	1022.02	23.08%	1	10	10	24	325	38.1	4.84	0.014	1.31	Downregulation
P48036	Annexin A5 GN = Anxa5	3863.46	76.49%	1	28	28	102	319	35.7	4.96	0.0063	1.21	Upregulation

Legend: 2T - two weeks after tumor cells inoculation.
Accession: UniProt number.
Description: Details about the protein including: name of the protein, gene name.
Score: Total score of the protein. This score is the sum of the scores of the individual peptides.
Coverage: The percentage of the protein sequence covered by identified peptides.
Proteins: The number of identified proteins in the protein group of a master protein.
Unique Peptides: The number of peptide sequences unique to a protein group.
Peptides: The number of unique peptide sequences.
PSMs: The total number of identified peptide sequences (peptide spectrum matches) for the protein, including those redundantly identified.
AAs: The sequence length of the protein.
MW: The calculated molecular weight of the protein.
Calc. pI: The theoretically calculated isoelectric point.
Average ratio: The ratio between the volumes of the spot between the compared images.

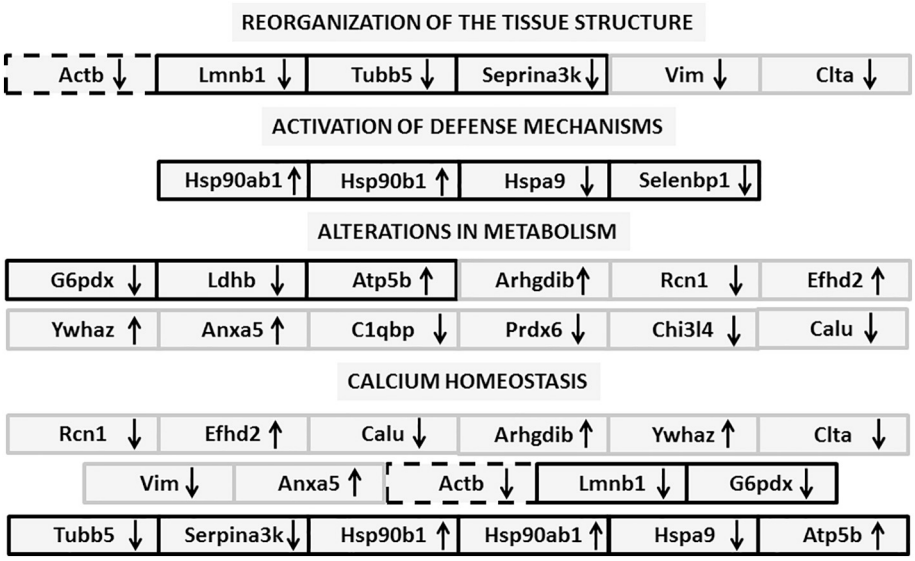

Fig. 5. Classification of differentially expressed proteins according to their functional relationships. The proteins were grouped into categories based on the information provided by the following programs/tools/databases: String DB, Panther DB, GeneMania, GeneOnthology, uniprot.org).
Legend: boxes with black outline - the proteins which showed differences in expression one week after tumor cell inoculation.
Boxes with gray outline - the proteins which showed differences in expression two weeks after tumor cell inoculation.
Box with dotted outline - the protein which showed differences in expression one and two weeks after tumor cell inoculation. (For interpretation of the references to color in this figure legend, the reader is referred to the web version of this article.)

primarily on the features of metastatic cancer cells (Li et al., 2006; Kischel et al., 2008). These studies, however, do not offer answers to the question of how healthy tissue is reorganized to attract cancer cells. Thus, the analysis of the target metastasis organs would be of high importance. Zheng et al. (2013) characterized the proteins related to the formation of lung metastatic niche (type VI collagen, HSP 90, fibrinogen) of colorectal cancer. Chen et al. (2004) identified 25 metastasis-related proteins involved in development of gastric cancer *e.g.* cytoskeletal proteins, stress-associated proteins and proteins involved in signal transduction, cell proliferation and differentiation along with metabolism. Although the results revealed the processes of metastasis-related changes, both analyses were performed in tissues with developed macrometastases, thus they did not facilitate characterization of early metastatic rearrangement of the tissue.

Our studies sought to define the early fingerprint of lung rearrangement before the development of multiple metastases. The proteomic changes during the early metastatic period were slight but significant. Indeed, the early functional changes were not expected to be extensive. Primary tumors were not yet palpable after the 1st week and formed in the 2nd week, and as reported by Suraj et al. (2019b), Smeda et al. (2018) and Chrabaszcz et al. (2018), the multiple metastases were formed in the following weeks after tumor inoculation. The early changes in the lungs in response to the presence of cancer cells and the onset of primary tumor development in the 1st week after tumor cell inoculation included especially the reorganization of the tissue (Actb, Lmnb1, Tubb5, Serpina3k) and activation of defense mechanisms (Selenbp1, Hsp90b1, Hsp90ab1, Hspa9), but also modifications in metabolic pathways (G6pdx, Atp5b, Ldhb). Further development of the solid tumor in the 2nd week after tumor cell inoculation, secretion of prolific tumor-derived factors as well as the presence of the circulating cancer cells further induced reorganization of the tissue (Actb, Vim, Clta), altering additional metabolic pathways (Anxa5, Arhgdib, C1qbp, Ywhaz, Prdx6, Chi3l4, Rcn1, Efhd2, Calu) and altered calcium signaling (Rcn1, Efhd2, Calu, Actb, Vim, Lmnb1, Clta, Tubb5, Serpina3k, Hsp90b1,Hsp90ab1, Hspa9. G6pdx, Atp5b, Anxa5, Arhgdib, Ywhaz).

Although 2D-DIGE technique used in this study represents a comprehensive tool that enables to define the changes in response to selected factor, and it overcomes the problems (variations and reproducibility) of classical two-dimensional polyacrylamide gel electrophoresis (2D-PAGE), still the detection and further identification of lower abundant proteins remains insufficient (Tannu and Hemby, 2006), what represents the limitation of the current study.

4.2.1. *Structural changes*

Early metastatic rearrangement of the tissue was evidenced by downregulation in expression of structural proteins. Disassembly of the cytoskeleton during the early metastatic period may originate from the elevation of 2-OH-E$^+$. Dalle-Donne et al. (2001) reported that actin was proposed to be the most sensitive constituent of the cytoskeleton to oxidative stress, leading to plasma membrane blebbing. Under high levels of oxidative stress, the actin cytoskeleton appears to play a protective role, accompanying the collapse of the actin cytoskeleton into oxidation-induced actin bodies (OABs) that sequesters actin and its associated proteins into immobile and non-dynamic structures (Farah et al., 2011; Pérez-Sala et al., 2015). Under oxidative stress, Vim cleavage (Chen et al., 2009) may lead to a lack of integrity in the vascular endothelium, impacting organization of proteins that are involved in adhesion, migration and cell signaling (Ivaska et al., 2007, Matveeva et al., 2010).

Reorganization of tissue structure may result from direct stimulation of cancer cells. Noteworthy is the lower expression of laminin observed in our experiment, which may reflect the onset of degradation of the basement membrane, leading to invasion of the lung tissue (Patarroyo et al., 2002). In our study Serpina3k was also downregulated early, pointing to early extracellular matrix (ECM) remodeling (Naba et al., 2017), potentially causing pro-angiogenic and pro-inflammatory changes in tissue structure, possibly promoting cancer cell metastasis (Yao et al., 2013).

4.2.2. *Calcium-related changes*

Many of the identified differentially expressed proteins are related to calcium [*e.g.,* Efhd2- Fan et al. (2017), Clta- Yao et al. (2012), Atp5b- Giorgio et al. (2017), Anxa- Sen et al. (1997), Rcn1- Suzuki et al. (2014); Xu et al. (2017), Calu- Mazzorana et al. (2016), Ywhaz- Ichimura et al. (2008), Arulpragasam et al. (2012), Arhgdib- Xiao et al. (2014), thus suggesting the importance of calcium signaling during the early onset of the disease. It seems like there is an interplay between proteins regulated or involved in the regulation of calcium.

Noted in the presented experiments, lower levels of Serpina3k (Zhang and Ma, 2008), Hspa9 (Li et al., 2018; Dudeja et al., 2009), Rcn-1 (Suzuki et al., 2014; Xu et al., 2017) and Calu (Sahoo et al., 2011) may result in calcium overload. In parallel, the observed loss of laminin reduces levels of calcium sensitivity (Chand et al., 2015). Importantly, high levels of calcium have been described to cause depolymerization of the microtubules and actin (Hepler, 2016, Nishimune et al., 2004) leading to reorganization of the tissue structure noted in our experiment.

On the other hand, the mechanisms involved in calcium removal were also activated. The observed depolymerization of actin filaments was reported to attenuate calcium release (Wang et al., 2002). In addition, downregulation of G6pdx noted in our study may be involved in decreasing levels of calcium (Gupte et al., 2011) and calcium channel activity (Rawat et al., 2012).

4.2.3. Proteomic changes in relation to formation of the tumor-promoting environment - the study on oxidative stress and NO-reflected endothelium dysfunction

The very early changes in the lung environment related to the progression of cancer were also revealed through the study of nitric oxide metabolites, a well-recognized parameters reflecting endothelial dysfunction. Tousoulis et al. (2012) confirmed that decreased production of NO in different pathological states causes serious problems in endothelial equilibrium and reflects the severity of endothelium dysfunction. The presented results suggest that the barrier function of the endothelium might be affected and enables the infiltration of immune cells and cancer cells to form metastases (Franses et al., 2013).

The apparent early development of oxidative stress may significantly induce the development of observed inflammation as reactive oxygen species (ROS) are believed to be responsible for secretion of pro- or anti-inflammatory molecules regulating the different steps in cancer development (Poillet-Perez et al., 2015). On the other hand, increased ROS may be secreted by immune cells increasingly noted in the lungs: TAM, mast cells, dendritic cells, natural killer (NK) cells, neutrophils, eosinophils and lymphocytes (Vendramini-Costa and Carvalho, 2012). In addition, observed in the presented experiments herein, degradation of nitric oxide may result from increased ROS generation, resulting in the formation of other ROS species, such as peroxynitrites (Fink et al., 2004). Elevated rates of ROS affect various processes, such as promoting tumor development and progression *e.g.*, cell proliferation, genetic instability, drug resistance (Pelicano et al., 2004), increasing vascular permeability, inducing trans-endothelial migration of tumor cells *via* stimulation of interleukin-8 and intracellular adhesion protein 1 (Roebuck, 1999), degrading ECM components (Kliment and Oury, 2010), activating Snail, thereby resulting in endothelial-mesenchymal transition (EndMT) (Djamali et al., 2005; Cannito et al., 2008) and, in consequence, lead to development of metastases. Downregulation of Serpina3k (Zhou et al., 2012), G6pdx (Wu et al., 2015), Ldha (Le et al., 2010) and Prdx (Rolfs et al., 2013) as well as upregulation of Arhgdib (Pastor et al., 2013), promotes and/or reflects the development of oxidative stress.

Oxidative stress significantly imposed to reorganization of tissue structure as described earlier. Additionally, ROS-related activation of the different mechanisms enabled the formation of tumor-promoting changes *e.g.* inhibition of cell death, lead to reduced sensitivity of cancer cells to hydrogen peroxide and ROS, enabled the protection of oncoproteins, reflected by alterations in Ywhaz (Pennington et al., 2018), Selenbp1 (Zhao et al., 2016), Hsp90 (Beck et al., 2009; Garcia-Cardena et al., 1998), Hspa9 (Yang et al., 2011), G6pdx (Efferth et al., 2006).

4.2.4. Metabolic shift and defense activation

The other changes related to formation of the tumor microenvironment and alterations in pathways regulating tumorigenesis, which lead to distant metastases formation, were observed in proteins involved in defense mechanisms - heat shock proteins, as well as Selenbp1. Changes in their concentration were reported to correlate with overall reduced survival (Cawthorn et al., 2012; Cheng et al., 2012; Zhang et al., 2013).

Some metabolic changes observed in our study might negatively affect lung function. The studies determined decreased levels of G6pdx, which may result in further EndMT (Wu et al., 2016), activates pro-inflammatory changes through oxidative stress and the NF-κB pathway (Yang et al., 2015). Noted loss of Prdx6 was described to enhance susceptibility to development of malignant tissue (Rolfs et al., 2013). Elevated Ywhaz was reported to activate pathways that promote tumor growth, sequestering tumor suppressing proteins and causing EndMT, poor prognosis and metastasis reoccurrence, contributing to the development of early cancer stages (Neal and Yu, 2010). Increased Atp5b as a binding partner of metastasis-related short peptide was reported to promote cancer metastasis (Li et al., 2017), whereas C1qbp reduction upregulated genes related to cell adhesion and invasion abilities (influencing p-GSK3/β-Catenin/L1CAM expression) (Wang et al., 2017).

On the other hand, some proteins seemed to act positively. Upregulation of Anxa5 was reported to suppress tumor angiogenesis (Zhang et al., 2017). It was shown that Arhgdib is a metastasis suppressor through Rho GTPases (Moissoglu et al., 2009). Ldhb was characterized as a molecular chaperone, and its reduced levels arrest the cell cycle, downregulating transcription (Valvona et al., 2016). Diminished levels of Ldha were shown to inhibit tumor progression (Le et al., 2010).

In conclusion, early metastatic rearrangement of the lungs is the prerequisite for the development of metastases. The tissue response is an interplay between pro- and anti-metastatic mechanisms accompanied by inflammation, oxidative stress and dysfunction of the barrier endothelial cells. This analysis enabled demonstration of the importance of calcium signaling during the early phase of metastasis development, early cytoskeleton and extracellular matrix reorganization, activation of defense mechanisms and metabolic adaptations.

Author contributions

Study design (AK, JS, MW), study execution (AK, JS, MW, EB, AZ, M. Stojak M. Sternak, AJ), interpretation of findings (AK, JS, MW), drafting the manuscript (AK, JS, MW), revising the manuscript (AK, JS, MW, EB, AZ, M. Stojak M. Sternak, AJ). All authors read and approved the final version of the manuscript.

Funding

The work was supported by National Science Centre, Poland (Narodowe Centrum Nauki, Polska) [MINIATURA project, JCET-UJ, DEC-2017/01/X/NZ5/00569] and partially by METENDOPHA project funded by The National Centre for Research and Development, Poland (Narodowe Centrum Badań i Rozwoju, Polska) (a grant coordinated by JCET-UJ, No. STRATEGMED1/233226/11/NCBR/2015).

Conflict of interest statement

The authors declare that there are no conflicts of interest.

Acknowledgements

The authors thank Joanna Wietrzyk (Ludwik Hirszfeld Institute of Immunology and Experimental Therapy, Polish Academy of Sciences, Wroclaw, Poland) for providing 4 T1 tumor cell line. We also thank Krystyna Wandzel (Jagiellonian Centre For Experimental Therapeutics, Krakow, Poland) for laboratory animal housekeeping and the Malopolska Centre of Biotechnology, Jagiellonian University, Krakow, Poland for providing the access to Typhoon Trio + Scanner and DeCyder 2D software v.7.2.

References

Arulpragasam, A., Magno, A.L., Ingley, E., Brown, S.J., Conigrave, A.D., Ratajczak, T., Ward, B.K., 2012. The adaptor protein 14-3-3 binds to the calcium-sensing receptor and attenuates receptor-mediated Rho kinase signalling. Biochem. J. 441 (3), 995–1006. https://doi.org/10.1042/BJ20111277.

Aslakson, C.J., Miller, F.R., 1992. Selective events in the metastatic process defined by analysis of the sequential dissemination of subpopulations of a mouse mammary tumor. Cancer Res. 52 (6), 1399–1405.

Bailey-Downs, L.C., Thorpe, J.E., Disch, B.C., Bastian, A., Hauser, P.J., Farasyn, T., Berry, W.L., Hurst, R.E., Ihnat, M.A., 2014. Development and characterization of a pre-clinical model of breast cancer lung micrometastatic to macrometastatic progression. PLoS One 9, 5. https://doi.org/10.1371/journal.pone.0098624.

Beck, R., Verrax, J., Gonze, T., Zappone, M., Pedrosa, R.C., Taper, H., Feron, O., Calderon, P.B., 2009. Hsp90 cleavage by an oxidative stress leads to its client proteins degradation and cancer cell death. Biochem. Pharmacol. 77 (3), 375–383. https://doi.org/10.1016/j.bcp.2008.10.019.

Biemar, F., Foti, M., 2013. Global progress against cancer—challenges and opportunities. Cancer Biol. Med. 10 (4), 183–186. https://doi.org/10.7497/j.issn.2095-3941.2013.04.001.

Blazejczyk, A., Papiernik, D., Porshneva, K., Sadowska, J., Wietrzyk, J., 2015. Endothelium and cancer metastasis: perspectives for antimetastatic therapy. Pharmacol. Rep. 67, 711–718. https://doi.org/10.1016/j.pharep.2015.05.014.

Brinton, L.T., Brentnall, T.A., Smith, J.A., Kelly, K.A., 2012. Metastatic biomarker discovery through proteomics. Cancer Genomics Proteomics 9 (6), 345–355.

Bryan, N.S., Grisham, M.B., 2007. Methods to detect nitric oxide and its metabolites in biological samples. Free Radic. Biol. Med. 43, 645–657. https://doi.org/10.1016/j.freeradbiomed.2007.04.026.

Buczek, E., Denslow, A., Mateuszuk, L., Proniewski, B., Wojcik, T., Sitek, B., Fedorowicz, A., Jasztal, A., Kus, E., Chmura-Skirlinska, A., Gurbiel, R., Wietrzyk, J., Chlopicki, S., 2018. Alterations in NO- and PGI2- dependent function in aorta in the orthotopic murine model of metastatic 4T1 breast cancer: relationship with pulmonary endothelial dysfunction and systemic inflammation. BMC Cancer 18 (1), 582. https://doi.org/10.1186/s12885-018-4445-z.

Cannito, S., Novo, E., Compagnone, A., di Bonzo, L.V., Busletta, Ch., Zamara, E., Paternostro, C., Povero, D., Bandino, A., Bozzo, F., Cravanzola, C., Bravoco, V., Colombatto, S., Parola, M., 2008. Redox mechanisms switch on hypoxia-dependent epithelial-mesenchymal transition in cancer cells. Carcinogenesis 29 (12), 2267–2278. https://doi.org/10.1093/carcin/bgn216.

Cawthorn, T.R., Moreno, J.C., Dharsee, M., Tran-Thanh, D., Ackloo, S., Zhu, P.H., Sardana, G., Chen, J., Kupchak, P., Jacks, L.M., Miller, N.A., Youngson, B.J., Iakovlev, V., Guidos, C.J., Vallis, K.A., Evans, K.R., McCready, D., Leong, W.L., Done, S.J., 2012. Proteomic analyses reveal high expression of decorin and endoplasmin (HSP90B1) are associated with breast cancer metastasis and decreased survival. PLoS One 7 (2), e30992. https://doi.org/10.1371/journal.pone.0030992.

Chand, K.K., Lee, K.M., Schenning, M.P., Lavidis, N.A., Noakes, P.G., 2015. Loss of β2-laminin alters calcium sensitivity and voltage-gated calcium channel maturation of neurotransmission at the neuromuscular junction. J. Physiol. 593 (1), 245–265. https://doi.org/10.1113/jphysiol.2014.284133.

Chen, J., Kähne, T., Röcken, Ch., Götze, H., Yu, J., Sung, J.J.Y., Chen, M., Hu, P., Malfertheiner, P., Ebert, M.P.A., 2004. Proteome analysis of gastric cancer metastasis by two-dimensional gel electrophoresis and matrix assisted laser desorption/ionization-mass spectrometry for identification of metastasis-related proteins. J. Proteome Res. 3, 1009–1016. https://doi.org/10.1021/pr049916l.

Chen, X., Kang, H., Zou, F., 2009. Low concentration of GA activates a preconditioning response in HepG2 cells during oxidative stress-roles of Hsp90 and vimentin. Cell Stress Chaperones 14, 381–389. https://doi.org/10.1007/s12192-008-0092-7.

Cheng, Q., Chang, J.T., Geradts, J., Neckers, L.M., Haystead, T., Spector, N.L., Lyerly, H.K., 2012. Amplification and high-level expression of heat shock protein 90 marks aggressive phenotypes of human epidermal growth factor receptor 2 negative breast cancer. Breast Cancer Res. 14 (2), R62. https://doi.org/10.1186/bcr3168.

Chrabaszcz, K., Jasztal, A., Smeda, M., Zielinski, B., Blat, A., Diem, M., Chlopicki, S., Malek, K., Marzec, K.M., 2018. Label-free FTIR spectroscopy detects and visualizes the early stage of pulmonary micrometastasis seeded from breast carcinoma. Biochim. Biophys. Acta Mol. basis Dis. 1864 (11), 3574–3584. https://doi.org/10.1016/j.bbadis.2018.08.022.

Crapo, J.D., Barry, B.E., Gehr, P., Bachofen, M., Weibel, E.R., 1982. Cell number and cell characteristics of the normal human lung. Am. Rev. Respir. Dis. 126 (2), 332–337. https://doi.org/10.1164/arrd.1982.126.2.332.

Dalle-Donne, I., Rossi, R., Milzani, A., Di Simplicio, P., Colombo, R., 2001. The actin cytoskeleton response to oxidants: from small heat shock protein phosphorylation to changes in the redox state of actin itself. Free Radic. Biol. Med. 31 (12), 1624–1632. https://doi.org/10.1016/S0891-5849(01)00749-3.

Djamali, A., Reese, S., Yracheta, J., Oberley, T., Hullett, D., Becker, B., 2005. Epithelial to mesenchymal transition and oxidative stress in chronic allograft nephropathy. Am. J. Transplant. 5 (3), 500–509. https://doi.org/10.1111/j.1600-6143.2004.00713.x.

Dorweiler, B., Torzewski, M., Dahm, M., Kirkpatrick, C.J., Lackner, K.J., Vahl, C.F., 2008. Subendothelial infiltration of neutrophil granulocytes and liberation of matrix-destabilizing enzymes in an experimental model of human neo-intima. Thromb. Haemost. 99 (2), 373–381. https://doi.org/10.1160/TH07-06-0387.

Dudeja, V., Mujumdar, N., Phillips, P., Chugh, R., Borja-Cacho, D., Dawra, R.K., Vickers, S.M., Saluja, A.K., 2009. Heat shock Ppotein 70 inhibits apoptosis in cancer cells through simultaneous and independent mechanisms. Gastroenterology 136 (5), 1772–1782. https://doi.org/10.1053/j.gastro.2009.01.070.

Efferth, T., Schwarzl, S.M., Smith, J., Osieka, R., 2006. Role of glucose-6-phosphate dehydrogenase for oxidative stress and apoptosis. Cell Death Differ. 13, 527–528. https://doi.org/10.1038/sj.cdd.4401807.

Fan, C.-C., Cheng, W.-C., Huang, Y.-C., Sher, Y.-P., Liou, N.-J., Chien, Y.-C., Lin, P.-S., Lin, P.-S., Chen, C.-H., Chang, W.-C., 2017. EFHD2 promotes epithelial-to-mesenchymal transition and correlates with postsurgical recurrence of stage I lung adenocarcinoma. Sci. Rep. 7, 14617. https://doi.org/10.1038/s41598-017-15186-y.

Farah, M.E., Sirotkin, V., Haarer, B., Kakhniashvili, D., Amberg, D.C., 2011. Diverse protective roles of the actin cytoskeleton during oxidative stress. Cytoskeleton (Hoboken) 68 (6), 340–354. https://doi.org/10.1002/cm.20516.

Fink, B., Laude, K., McCann, L., Doughan, A., Harrison, D.G., Dikalov, S., 2004. Detection of intracellular superoxide formation in endothelial cells and intact tissues using dihydroethidium and an HPLC-based assay. Am. J. Physiol. Cell Physiol. 287 (4), C895–C904. https://doi.org/10.1152/ajpcell.00028.2004.

Franses, J.W., Drosu, N.C., Gibson, W.J., Chitalia, V.C., Edelman, E.R., 2013. Dysfunctional endothelial cells directly stimulate cancer inflammation and metastasis. Int. J. Cancer 133, 1334–1344. https://doi.org/10.1002/ijc.28146.

Garcia-Cardena, G., Fan, R., Shah, V., Sorrentino, R., Cirino, G., Papapetropoulos, A., Sessa, W.C., 1998. Dynamic activation of endothelial nitric oxide synthase by Hsp90. Nature 392, 821–824. https://doi.org/10.1038/33934.

Giorgio, V., Burchell, V., Schiavone, M., Bassot, C., Minervini, G., Petronilli, V., Argenton, F., Forte, M., Tosatto, S., Lippe, G., Bernardi, P., 2017. Ca(2+) binding to F-ATP synthase beta subunit triggers the mitochondrial permeability transition. EMBO Rep. 18 (7), 1065–1076. https://doi.org/10.15252/embr.201643354.

Gray, P., 1954. The Microtomist's Formulary and Guide. Blakiston Edition, New York.

Gundry, R.L., White, M.Y., Murray, C.I., Kane, L.A., Fu, Q., Stanley, B.A., Van Eyk, J.E., 2009. Preparation of proteins and peptides for mass spectrometry analysis in a bottom-up proteomics workflow. Curr. Protoc. Mol. Biol. 10, 10.25.1–10.25.23. https://doi.org/10.1002/0471142727.mb1025s88.

Gupte, R.S., Ata, H., Rawat, D., Abe, M., Taylor, M.S., Ochi, R., Gupte, S.A., 2011. Glucose-6-phosphate dehydrogenase is a regulator of vascular smooth muscle contraction. Antioxid. Redox Signal. 14 (4), 543–558. https://doi.org/10.1089/ars.2010.3207.

Hepler, P., 2016. The cytoskeleton and its regulation by calcium and protons. Plant Physiol. 170 (1), 3–22. https://doi.org/10.1104/pp.15.01506.

Ho, J., Kong, J.W., Choong, L.Y., Loh, M.C., Toy, W., Chong, P.K., Wong, C.H., Wong, C.Y., Shah, N., Lim, Y.P., 2009. Novel breast cancer metastasis-associated proteins. J. Proteome Res. 8 (2), 583–594. https://doi.org/10.1021/pr8007368.

Ichimura, T., Taoka, M., Hozumi, Y., Goto, K., Tokumitsu, H., 2008. 14-3-3 proteins directly regulate Ca^{2+}/calmodulin-dependent protein kinase kinase α through phosphorylation-dependent multisite binding. FEBS Lett. 582 (5), 661–665. https://doi.org/10.1016/j.febslet.2008.01.037.

Ivaska, J., Pallari, H.M., Nevo, J., Eriksson, J.E., 2007. Novel functions of vimentin in cell adhesion, migration, and signaling. Exp. Cell Res. 313, 2050–2062. https://doi.org/10.1016/j.yexcr.2007.03.040.

Jablonska, J., Lang, S., Sionov, R.V., Granot, Z., 2017. The regulation of pre-metastatic niche formation by neutrophils. Oncotarget 8 (67), 112132–112144. https://doi.org/10.18632/oncotarget.22792.

Kischel, P., Guillonneaeu, F., Dumont, B., Bellahcène, A., Stresing, V., Clézardin, P., De Pauw, E.A., Castronovo, V., 2008. Cell membrane proteomic analysis identifies proteins differentially expressed in osteotropic human breast cancer cells. Neoplasia 10 (9), 1014–1020. https://doi.org/10.1593/neo.08570.

Kliment, C.R., Oury, T.D., 2010. Oxidative stress, extracellular matrix targets, and idiopathic pulmonary fibrosis. Free Radic. Biol. Med. 49 (5), 707–717. https://doi.org/10.1016/j.freeradbiomed.2010.04.036.

Langley, R.R., Fidler, I.J., 2011. The seed and soil hypothesis revisited-the role of tumour-stroma interactions in metastasis to different organs. Int. J. Cancer 128, 2527–2535. https://doi.org/10.1002/ijc.26031.

Le, A., Cooper, C.R., Gouw, A.M., Dinavahi, R., Maitra, A., Deck, L.M., Royer, R.E., Jagt, D.L.V., Semenza, G.L., Dang, C.V., 2010. Inhibition of lactate dehydrogenase a induces oxidative stress and inhibits tumor progression. Proc. Natl. Acad. Sci. U. S. A. 107 (5), 2037–2042. https://doi.org/10.1073/pnas.0914433107.

Li, D.Q., Wang, L., Fei, F., Hou, Y.F., Luo, J.M., Wei-Chen, Zeng, R., Wu, J., Lu, J.S., Di, G.H., Ou, Z.L., Xia, Q.C., Shen, Z.Z., Shao, Z.M., 2006. Identification of breast cancer metastasis-associated proteins in an isogenic tumour metastasis model using two-dimensional gel electrophoresis and liquid chromatography-ion trap-mass spectrometry. Proteomics 6 (11), 3352–3368. https://doi.org/10.1002/pmic.200500617.

Li, W., Li, Y., Li, G., Zhou, Z., Chang, X., Xia, Y., Dong, X., Liu, Z., Ren, B., Liu, W., Li, Y., 2017. Ectopic expression of the ATP synthase β subunit on the membrane of PC-3M cells supports its potential role in prostate cancer metastasis. Int. J. Oncol. 50 (4), 1312–1320. https://doi.org/10.3892/ijo.2017.3878.

Li, C., Sunderic, K., Nicoll, S.B., Wang, S., 2018. Downregulation of heat shock protein 70 impairs osteogenic and chondrogenic differentiation in human mesenchymal stem cells. Sci. Rep. 8, 553. https://doi.org/10.1038/s41598-017-18541-1.

Liu, Y., Cao, X., 2016. Characteristics and significance of the pre-metastatic niche. Cancer Cell 30 (5), 668–681. https://doi.org/10.1016/j.ccell.2016.09.011.

Maru, Y., 2015. The lung metastatic niche. J. Mol. Med (Berl). 93, 1185–1192. https://doi.org/10.1007/s00109-015-1355-2.

Matveeva, E.A., Chernoivanenko, I.S., Minin, A.A., 2010. Vimentin intermediate filaments protect mitochondria from oxidative stress. Biochem. (Mosc.) Suppl. Ser. A: Membr. Cell Biol. 4 (4), 321–331. https://doi.org/10.1134/S199074781004001X.

Mazzorana, M., Hussain, R., Sorensen, T., 2016. Ca-dependent folding of human calumenin. PLoS One 11 (3), e0151547. https://doi.org/10.1371/journal.pone.0151547.

Moissoglu, K., McRoberts, K.S., Meier, J.A., Theodorescu, D., Schwartz, M.A., 2009. RhoGDI2 suppresses metastasis via unconventional regulation of RhoGTPases. Cancer Res. 69 (7), 2838–2844. https://doi.org/10.1158/0008-5472.CAN-08-1397.

Naba, A., Clauser, K.R., Mani, D.R., Carr, S.A., Hynes, R.O., 2017. Quantitative proteomic profiling of the extracellular matrix of pancreatic islets during the angiogenic switch and insulinoma progression. Sci. Rep. 7, 40495. https://doi.org/10.1038/srep40495.

Neal, C.L., Yu, D., 2010. 14-3-3ζ as a prognostic marker and therapeutic target for cancer. Expert. Opin. Ther. Targets 14 (12), 1343–1354. https://doi.org/10.1517/14728222.2010.531011.

Nishimune, H., Sanes, J.R., Carlson, S.S., 2004. A synaptic laminin-calcium channel interaction organizes active zones in motor nerve terminals. Nature 432 (7017), 580–587. https://doi.org/10.1038/nature03112.

Paget, S., 1989. The distribution of secondary growths in cancer of the breast. Lancet 1, 571–573. https://doi.org/10.1016/S0140-6736(00)49915-0.

Pastor, M.D., Nogal, A., Molina-Pinelo, A., Meléndez, R., Romero-Romero, B., Mediano, M.D., López-Campos, J.L., García-Carbonero, R., Sanchez-Gastaldo, A., Carnero, A., Paz-Ares, L., 2013. Identification of oxidative stress related proteins as biomarkers for lung cancer and chronic obstructive pulmonary disease in bronchoalveolar lavage. Int. J. Mol. Sci. 14, 3440–3455. https://doi.org/10.3390/ijms14023440.

Patarroyo, M., Tryggvason, K., Virtanen, I., 2002. Laminin isoforms in tumor invasion, angiogenesis and metastasis. Semin. Cancer Biol. 12 (3), 197–207. https://doi.org/10.1016/S1044-579X(02)00023-8.

Pelicano, H., Carney, D., Huang, P., 2004. ROS stress in cancer cells and therapeutic implications. Drug Resist. Updat. 7 (2), 97–110. https://doi.org/10.1016/j.drup.2004.01.004.

Pennington, K.L., Chan, T.Y., Torres, M.P., Andersen, J.L., 2018. The dynamic and stress-adaptive signaling hub of 14-3-3: emerging mechanisms of regulation and context-dependent protein-protein interactions. Oncogene 37 (42), 5587–5604. https://doi.org/10.1038/s41388-018-0348-3.

Pérez-Sala, D., Oeste, C.L., Martínez, A.E., Carrasco, J., Garzón, B., Cañada, F.J., 2015. Vimentin filament organization and stress sensing depend on its single cysteine residue and zinc binding. Nat. Commun. 6, 7287. https://doi.org/10.1038/ncomms8287.

Poillet-Perez, L., Despouy, G., Delage-Mourroux, R., Boyer-Guittaut, M., 2015. Interplay between ROS and autophagy in cancer cells, from tumor initiation to cancer therapy. Redox Biol. 4, 184–192. https://doi.org/10.1016/j.redox.2014.12.003.

Powell, D.R., Huttenlocher, A., 2016. Neutrophils in the tumor microenvironment. Trends Immunol. 37 (1), 41–52. https://doi.org/10.1016/j.it.2015.11.008.

Psaila, B., Lyden, D., 2009. The metastatic niche: adapting the foreign soil. Nat. Rev. Cancer 9, 285–293. https://doi.org/10.1038/nrc2621.

Pulaski, B.A., Ostrand-Rosenberg, S., 2001. Mouse 4T1 breast tumour model. Curr. Protoc. Immunol. 20https://doi.org/10.1002/0471142735.im2002s39. 20.2.1-20.2.16.

Quail, D.F., Joyce, J.A., 2013. Microenvironmental regulation of tumor progression and metastasis. Nat. Med. 19, 1423–1437. https://doi.org/10.1038/nm.3394.

Rawat, D.K., Hecker, P., Watanabe, M., Chettimada, S., Levy, R.J., Okada, T., Edwards, J.G., Gupte, S.A., 2012. Glucose-6-phosphate dehydrogenase and NADPH redox regulates cardiac myocyte L-type calcium channel activity and myocardial contractile function. PLoS One 7 (10), e45365. https://doi.org/10.1371/journal.pone.0045365.

Roebuck, K.A., 1999. Oxidant stress regulation of IL-8 and ICAM-1 gene expression: differential activation and binding of the transcription factors AP-1 and NF-kappaB (review). Int. J. Mol. Med. 4 (3), 223–230. https://doi.org/10.3892/ijmm.4.3.223.

Rolfs, F., Huber, M., Gruber, F., Böhm, F., Pfister, H.J., Bochkov, V.N., Tschachler, E., Dummer, R., Hohl, D., Schäfer, M., Werner, S., 2013. Dual role of the antioxidant enzyme peroxiredoxin 6 in skin carcinogenesis. Cancer Res. 73 (11), 3460–3469. https://doi.org/10.1158/0008-5472.CAN-12-4369.

Sahoo, S.K., Seo, I.-R., Kim, T., Kim, D.H., 2011. Calumenin inhibits Ca^{2+} release from sarcoplasmic reticulum in murine cardiomyocytes through a direct interaction with RyR2. Biophys. J. 100 (3), 289A–290A. https://doi.org/10.1016/j.bpj.2010.12.1785.

Sceneay, J., Smyth, M.J., Möller, A., 2013. The pre-metastatic niche: finding common ground. Cancer Metastasis Rev. 32 (3–4), 449–464. https://doi.org/10.1007/s10555-013-9420-1.

Sen, N., Spitzer, A.R., Chander, A., 1997. Calcium-dependence of synexin binding may determine aggregation and fusion of lamellar bodies. Biochem. J. 322, 103–109 Pt 1.

Shevchenko, A., Wilm, E., Vorm, O., Mann, M., 1996. Mass spectrometric sequencing of proteins silver-stained polyacrylamide gels. Anal. Chem. 68 (5), 850–858. https://doi.org/10.1021/ac950914h.

Smeda, M., Kieronska, A., Adamski, M.G., Proniewski, B., Sternak, M., Mohaissen, T., Przyborowski, K., Derszniak, K., Kaczor, D., Stojak, M., Buczek, E., Jasztal, A., Wietrzyk, J., Chlopicki, S., 2018. Nitric oxide deficiency and endothelial-mesenchymal transition of pulmonary endothelium in the progression of 4T1 metastatic breast cancer in mice. Breast Cancer Res. 20 (1), 86. https://doi.org/10.1186/s13058-018-1013-z.

Suraj, J., Kurpińska, A., Olkowicz, M., Niedzielska-Andres, E., Smolik, M., Zakrzewska, A., Jasztal, A., Sitek, B., Chlopicki, S., Walczak, M., 2018. Development, validation and application of a micro-liquid chromatography-tandem mass spectrometry based method for simultaneous quantification of selected protein biomarkers of endothelial dysfunction in murine plasma. J. Pharm. Biomed. Anal. 149, 465–474. https://doi.org/10.1016/j.jpba.2017.11.023.

Suraj, J., Kurpińska, A., Sternak, M., Smolik, M., Niedzielska-Andres, E., Zakrzewska, A., Chlopicki, S., Walczak, M., 2019a. Quantitative measurement of selected protein biomarkers of endothelial dysfunction by micro-liquid chromatography-tandem mass spectrometry based on stable isotope dilution method. Talanta 194, 1005–1016. https://doi.org/10.1016/j.talanta.2018.10.067.

Suraj, J., Kurpinska, A., Zakrzewska, A., Sternak, M., Stojak, M., Jasztal, A., Walczak, M., Chlopicki, S., 2019b. Endothelial dysfunction in early and late breast cancer metastasis assessed by simultaneous quantification of endothelial biomarkers using a mass spectrometry-based method. Dis. Models Mech. https://doi.org/10.1242/dmm.036269. (in press).

Suzuki, N., Ban, S., Itoh, E., Chen, S., Imai, F.L., Sawano, Y., Miyakawa, T., Tanokura, M., Yonezawa, N., 2014. Calcium-dependent structural changes in human reticulocalbin-1. J. Biochem. 155 (5), 281–293. https://doi.org/10.1093/jb/mvu003.

Tannu, N.S., Hemby, S.E., 2006. Two-dimensional fluorescence difference gel electrophoresis for comparative proteomics profiling. Nat. Protoc. 1 (4), 1732–1742. https://doi.org/10.1038/nprot.2006.256.

Tousoulis, D., Kampoli, A.M., Tentolouris, C., Papageorgiou, N., Stefanadis, C., 2012. The role of nitric oxide on endothelial function. Curr. Vasc. Pharmacol. 10, 4–18. https://doi.org/10.2174/157016112798829760.

Valvona, C.J., Fillmore, H.L., Nunn, P.B., Pilkington, G.J., 2016. The regulation and function of lactate dehydrogenase a: therapeutic potential in brain tumor. Brain Pathol. 26 (1), 3–17. https://doi.org/10.1111/bpa.12299.

Vendramini-Costa, D.B., Carvalho, J.E., 2012. Molecular link mechanisms between inflammation and cancer. Curr. Pharm. Des. 18 (26), 3831–3852. https://doi.org/10.2174/138161212802083707.

Walczak, M., Suraj, J., Kuś, K., Kij, A., Zakrzewska, A., Chłopicki, S., 2015. Towards a comprehensive endothelial biomarkers profiling and endothelium-guided pharmacotherapy. Pharmacol. Rep. 67, 771–777. https://doi.org/10.1016/j.pharep.2015.06.008.

Wang, Y., Mattson, M.P., Furukawa, K., 2002. Endoplasmic reticulum calcium release is modulated by actin polymerization. J. Neurochem. 82 (4), 945–952. https://doi.org/10.1046/j.1471-4159.2002.01059.x.

Wang, Y., Fu, D., Su, J., Chen, Y., Qi, C., Sun, Y., Niu, Y., Zhang, N., Yue, D., 2017. C1QBP suppresses cell adhesion and metastasis of renal carcinoma cells. Sci. Rep. 7, 999. https://doi.org/10.1038/s41598-017-01084-w.

Weigelt, B., Peterse, J.L., van't Veer, L.J., 2005. Breast cancer metastasis: markers and models. Nat. Rev. Cancer 5, 591–602. https://doi.org/10.1038/nrc1670.

Wu, Y.-H., Chiu, D.T.-Y., Lin, H.-R., Tang, H.-Y., Cheng, M.-L., Ho, H.-Y., 2015. Glucose-6-phosphate dehydrogenase enhances antiviral response through downregulation of NADPH sensor HSCARG and upregulation of NF-κB signaling. Viruses 7 (12), 6689–6706. https://doi.org/10.3390/v7122966.

Wu, Y.-H., Lee, Y.-H., Chiu, D.T.-Y., 2016. Knockdown glucose-6-phosphate dehydrogenase promotes EMT through downregulation of E-cadherin by miR-200b inhibition in A549 cells. FASEB J. 30 (Suppl.1), 50.5.

Xiao, K., Wang, Y., Chang, Z., Lao, Y., Chang, D.C., 2014. p32, a novel binding partner of Mcl-1, positively regulates mitochondrial Ca(2+) uptake and apoptosis. Biochem. Biophys. Res. Commun. 451 (2), 322–328. https://doi.org/10.1016/j.bbrc.2014.07.122.

Xu, S., Xu, Y., Chen, L., Fang, Q., Song, S., Chen, J., Teng, J., 2017. RCN1 suppresses ER stress-induced apoptosis via calcium homeostasis and PERK-CHOP signaling. Oncogene 6, e304. https://doi.org/10.1038/oncsis.2017.6.

Yang, H., Zhou, X., Liu, X., Yang, L., Chen, Q., Zhao, D., Zuo, J., Liu, W., 2011. Mitochondrial dysfunction induced by knockdown of mortalin is rescued by Parkin. Biochem. Biophys. Res. Commun. 410 (1), 114–120. https://doi.org/10.1016/j.bbrc.2011.05.116.

Yang, H.-C., Cheng, M.-L., Hua, Y.-S., Wu, Y.-H., Lin, H.-R., Liu, H.-Y., Ho, H.-Y., Chiu, D.T.-Y., 2015. Glucose 6-phosphate dehydrogenase knockdown enhances IL-8 expression in HepG2 cells via oxidative stress and NF-κB signaling pathway. J. Inflamm. (Lond). 12 (1), 34. https://doi.org/10.1186/s12950-015-0078-z.

Yao, Y., Huang, X., Gu, X., Xu, Z., Zhang, Y., Huang, L., Li, S., Dai, Z., Ci, C., Zhou, T., Cai, W., Yang, Z., Gao, G., Yang, X., 2013. SERPINA3K induces apoptosis in human colorectal cancer cells via activating the Fas/FasL/caspase-8 signaling pathway. FEBS J. 280 (14), 3244–3255. https://doi.org/10.1111/febs.12303.

Yao, L.-H., Rao, Y., Varga, K., Wang, C.-Y., Xiao, P., Lindau, M., Gong, L.-W., 2012. Synaptotagmin 1 is necessary for the Ca^{2+} dependence of clathrin-mediated endocytosis. J. Neurosci. 32 (11), 3778–3785. https://doi.org/10.1523/JNEUROSCI.3540-11.2012.

Zhang, M., Ma, J.-X., 2008. SERPINA3K prevents oxidative stress induced necrotic cell death by inhibiting calcium overload. PLoS One 3 (12), e4077. https://doi.org/10.1371/journal.pone.0004077.

Zhang, S., Li, F., Younes, M., Liu, H., Chen, Ch., Yao, Q., 2013. Reduced selenium-binding protein 1 in breast cancer correlates with poor survival and resistance to the antiproliferative effects of selenium. PLoS One 8 (5), e63702. https://doi.org/10.1371/journal.pone.0063702.

Zhang, X., Huo, L., Jin, H., Han, Y., Wang, J., Zhang, Y., Lai, X., Le, Z., Zhang, J., Hua, Z., 2017. Anti-cancer activity of Annexin V in murine melanoma model by suppressing tumor angiogenesis. Oncotarget 8 (26), 42602–42612. https://doi.org/10.18632/oncotarget.16645.

Zhao, C., Zeng, H., Wu, R.T.Y., Cheng, W.-H., 2016. Loss of selenium-binding protein 1 decreases sensitivity to clastogens and intracellular selenium content in HeLa cells. PLoS One 11 (7), e0158650. https://doi.org/10.1371/journal.pone.0158650.

Zheng, Y., Lin, Y., Situ, D., Jiang, L., Su, X., Long, H., 2013. Analysis of differentially expressed proteins involved in metastatic niche of lung. Thoracic Cancer 4, 385–394. https://doi.org/10.1111/1759-7714.12033.

Zhou, T., Zong, R., Zhang, Z., Zhu, C., Pan, F., Xiao, X., Liu, Z., He, H., Ma, J.-X., Liu, Z., Zhou, Y., 2012. SERPINA3K protects against oxidative stress via modulating ROS generation/degradation and KEAP1-NRF2 pathway in the corneal epithelium. Invest. Ophthalmol. Vis. Sci. 53 (8), 5033–5043. https://doi.org/10.1167/iovs.12-9729.

Zielonka, J., Vasquez-Vivar, J., Kalyanaraman, B., 2008. Detection of 2-hydroxyethidium in cellular systems: a unique marker product of superoxide and hydroethidine. Nat. Protoc. 3, 8–21. https://doi.org/10.1038/nprot.2007.473.